Supersolidus Liquid Phase Sintering Modeling of Inconel 718 Superalloy

DAVID LEVASSEUR and MATHIEU BROCHU

Powder metallurgy of Inconel 718 superalloy is advantageous as a near-net shape process for complex parts to reduce the buy-to-fly ratio and machining cost. However, sintering Inconel 718 requires the assistance of supersolidus liquid formation to achieve near full density and involves the risk of distortion at high temperatures. The present work is focused on modeling the onset of sintering and distortion as a function of temperature, grain size, and part geometry for Inconel 718. Using experimental sintering results and data available in the literature, the supersolidus liquid phase sintering of Inconel 718 was modeled. The model was used to define a processing window where part distortion would be avoided.

I. INTRODUCTION

POWDER injection molding (PIM) and binder jetting (BJ) additive manufacturing (AM) routes[1] are key avenues to fabricate complex parts, and more advantageous for high strength and specialty alloys. The PIM and BJ routes involve the mandatory use of a binder to create the green compact either under a molding action or *via* a layer-by-layer approach, followed by a sintering cycle. Some of the benefits of these near-net shape routes include the sustainable raw material usage, lower energy consumption, and limiting the difficulties associated with machining operations. These processing advantages explain the surge of research on these processes for the Inconel systems[2–12] for high temperature applications including turbines (jet engine, energy production), pumps, or rocket motors.[13]

The primary drawback of these approaches for Inconel 718 resides in the low sinterability of the green compact. Since Inconel 718 mass transport processes are limited at temperatures lower than solidus, it is not practical to sinter the alloy to full density in the solid state. Typical industrial practices, to reach mechanical properties equivalent or superior to that of wrought counterparts, involve a two-step process where sintering is initially carried out followed by hot isostatic pressing (HIP) as the final step.[6,8–12] This first sintering step can be associated with distortion,[14,15] defeating the advantage of the near-net shape approach. As such, a careful understanding of the sintering cycle is necessary to control the competitive interaction between maximizing density and minimizing distortion.

Nickel-based superalloys are often sintered in the semisolid regime, a technique also called supersolidus liquid phase sintering (SLPS).[6,10] The development of a liquid phase during sintering causes rapid shrinkage of the part and is used by many to achieve close to full density with Inconel 718 powders.[3–6,8–12] Shape retention during SLPS was studied by Liu *et al.*[14] They modeled the distribution of the liquid phase in the compacted powder microstructure and were able to predict the onset of sintering and distortion based on the physical properties of the powder and the sintering temperature. Their model is described in the following section.

A. *The SLPS Model*

The effect of the liquid formation on the compacted powder part is directly related to the structure of the part, in essence the powder particle size and the grain size of the powder. The liquid first covers grain boundaries and disrupts particle cohesion leading to a rearrangement of the grains driven by capillary forces and liquid flow under pressure gradients.[14,16,17] The rigidity of the part is assumed to be mainly linked to the extent of solid bonds between grains. The liquid film at grain boundaries may act as a lubricant for grain sliding, but can also maintain the cohesion between grains by its viscous resistance to deformation.[14] The understanding of the distribution of liquid on grain boundaries is thus the first step in assessing the rigidity of the compacted powder.

The coverage of solid grains by liquid (F_C) was described by Campbell[18] with a simple model using the liquid volume fraction (V_L) and the dihedral angle (ϕ) as shown in Eqs. [1] and [2]:

$$F_C = 2.64 \left(\frac{V_L}{a} \right)^{1/2} \quad [1]$$

DAVID LEVASSEUR, R&D Project Manager, is with the Quebec Metallurgy Center, Cegep de Trois-Rivières, 3095 Westinghouse Street, Trois-Rivières G9A 5E1, Canada. MATHIEU BROCHU, Associate Professor, is with the Department of Mining and Materials Engineering, McGill University, 3610 University Street, Montreal H3A 0C5, Canada. Contact e-mail: Mathieu.brochu@mcgill.ca

$$a = \sqrt{3} + \frac{3}{\tan[30 - (\phi/2)]} - \left[\frac{30 - (\phi/2)}{60}\right] \frac{\pi}{\sin^2[30 - (\phi/2)]}$$
$$[2]$$

The model was used by Liu et al.[14] to define the contiguity of the semisolid structure (C_{SS}) as per Eq. [3]:

$$C_{SS} = 1 - F_C. \qquad [3]$$

They further used a geometrical relationship to link the thickness of the grain boundary liquid film (δ) with the contiguity, the average grain size (G), and the liquid volume fraction using Eq. [4]:

$$\delta(1 - C_{SS}) = \frac{G}{3} \frac{V_L}{(1 - V_L)}. \qquad [4]$$

This equation states that the grain boundary liquid film thickens when either the liquid fraction or grain size increases. In turn, an increase in liquid film thickness reduces the viscous resistance of said film as expressed by Eq. [5]:

$$R = \frac{\eta_L v A^2}{\delta^3}, \qquad [5]$$

where R is the force of the resistance to movement between two grains, η_L is the viscosity of the liquid phase, v is the relative velocity of the two grains, and A is the area of the grain faces.

The liquid film viscous force combined with the resistance of the solid contacts between grains (σ_{SS}) defines the bond strength between two grains as shown in Eq. [6]:

$$F_{bond} = \pi G^2 \sigma_{SS} C_{SS} + \frac{\alpha \eta_L \pi G^4 (1 - C_{SS})^2}{\delta^3}, \qquad [6]$$

where πG^2 is the surface area of a grain and α is a constant with units of velocity. Equation [6] is used to define the rigidity of the compacted powder part with the first term expressing the resistance of the solid contacts and the second term relating to the viscous resistance of the liquid film between grains.[14]

Two forces acts on the grains during sintering, namely the capillary force and gravity. The former is responsible for the shrinkage of the porous part, while the latter is responsible for the distortion of the semisolid part. The onset of shrinkage occurs when the capillary force becomes larger than the bonding force; and in the same way, the onset of distortion occurs when the gravitational force is higher than the resistance of the part. The capillary force acting on grains separated by a liquid film has been studied by Liu et al.[19] and is estimated by Eq. [7]:

$$\sigma = \frac{5.2\gamma_{LV} \cos\theta}{D\left(1 - (\rho_g/\rho)^{1/3}\right)}, \qquad [7]$$

where γ_{LV} is the liquid–vapor surface energy, θ is the wetting angle (assumed to be 0 deg), D is the mean

particle diameter, and ρ and ρ_g are the density of the part and the green density, respectively. The densification during SLPS is driven by the shear stress which is half the capillary stress between two grains.[17] Thus, to take into account the shear stress and the force acting on the grains, Eq. [8] is used:

$$F_{max} = \frac{2.6\gamma_{LV} \cos\theta}{D\left(1 - (\rho_g/\rho)^{1/3}\right)} \pi G^2. \qquad [8]$$

The gravitational force on the other hand is expressed by Eq. [9]:

$$F_G = \frac{\rho g h}{2}, \qquad [9]$$

where F_G is the maximum shear force caused by gravity on the bottom grains of a part with height h and density ρ.

Comparing Eqs. [8] and [9] with Eq. [6], Liu et al.[14] defined two criteria for the onset of sintering and onset of distortion, respectively. Since the rigidity of the part is related to the liquid film thickness, Eq. [4] is also used to define the criteria. The reader is referred to the work of Liu et al. for a complete demonstration of the model, as only the criteria are presented here in Eqs. [10] to [12]:

$$\xi_{densif} = \left(\frac{\alpha\eta_L}{\sigma_{SS}}\right)^{1/3} \frac{(1 - C_{SS})^{5/3}}{(A - C_{SS})^{1/3}}, \quad A = \frac{2.6\gamma_{LV} \cos\theta}{D\left(1 - (\rho_g/\rho)^{1/3}\right)} \frac{1}{\sigma_{SS}}$$
$$[10]$$

$$\xi_{distort} = \left(\frac{\alpha\eta_L}{\sigma_{SS}}\right)^{1/3} \frac{(1 - C_{SS})^{5/3}}{(B - C_{SS})^{1/3}}, \quad B = \frac{\rho g h}{2} \frac{1}{\sigma_{SS}} \quad [11]$$

$$\xi = \frac{G^{1/3}}{3} \frac{V_L}{(1 - V_L)}, \qquad [12]$$

where ξ_{densif} is the criterion for the onset of sintering, $\xi_{distort}$ is the criterion for the onset of distortion, and ξ is the softening parameter. Therefore, when $\xi \geq \xi_{densif}$, the shrinkage is initiated, and when $\xi \geq \xi_{distort}$ distortion of the part occurs.

The objective of this paper is to combine experimental data and reported values to propose a unified SLPS model, delineating the processing window for Inconel 718. The experimental data and relationships generated for this work include the liquid fraction evolution with temperature, the densification, and the grain size for different sintering cycles. The proposed model, which accounts for the effects of the microstructure and the part geometry, was able to predict the onset of sintering and distortion from analysis of the rigidity of the semisolid system.
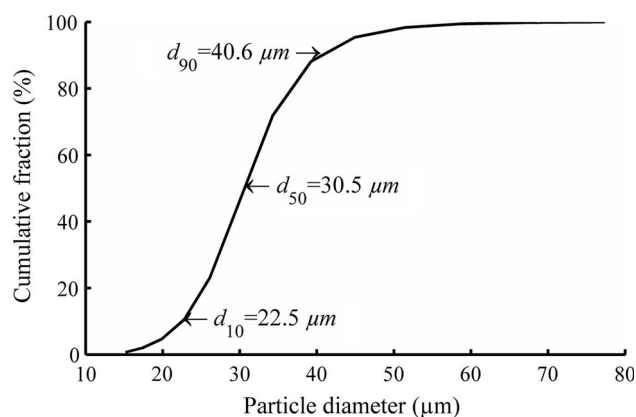
II. EXPERIMENTAL METHODS

The Inconel 718 powder used in this study was provided by Sulzer Metco, under the trade name of AMDRY 1718. The powder composition, as provided

Table I. Chemical Analysis of the AMDRY 1718 Powder

	Al	C	Co	Cr	Fe	Nb	Ni	Mo	Ti	O
Weight percent	0.43	0.05	0.09	19.11	17.92	5.07	53.07	3.13	0.94	0.02
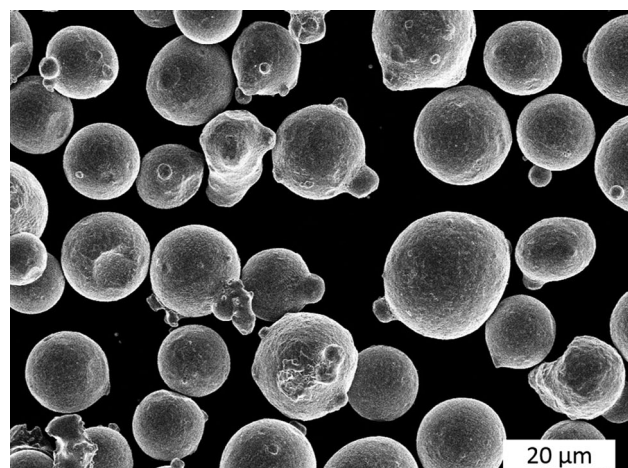
Fig. 1—(a) SEM image of the powder and (b) particle size analysis.

by the manufacturer, is listed in Table I. A scanning electron microscope (JEOL JSM-820) image of the powder is shown in Figure 1(a). The particle size distribution was measured on a 10 g sample by laser interferometry using a Horiba LA-920 Particle Size Analyzer, using isopropanol as the particle carrier, and the particle size cumulative frequency graph is presented in Figure 1(b).

The multi-melting events were measured using differential scanning calorimetry (DSC) of the powder in a Netzsch TGA/DSC (STA-449-F3), with a scanning interval from room temperature to 1533 K (1260 °C) using a heating rate of 10 K/min under a flowing argon atmosphere. Calibration of the DSC temperature and enthalpy was done with 99.99 pct purity indium, copper, and nickel. The contribution of the heat capacity from the sample and crucible is subtracted from the heat balance equation (Eq. [13]) by calibration and baseline fitting which is commonly used for DSC analysis.[20]

$$Q_{\text{melting}} = V_1 m_{\text{sample}} \Delta H, \qquad [13]$$

where Q_{melting} is the heat (Joules) measured by DSC after correction of the DSC trace, m_{sample} is the sample mass, and ΔH is the latent heat of fusion.

The preparation of compacts was done using a slip casting technique described by Hajmrle and Anger.[4] The slip casting slurry was prepared with 60 vol pct solid loading using a 1 wt pct ammonium alginate aqueous solution as the binder. The slurry was cast in plaster molds to obtain cylindrical samples with a diameter of 2.5 cm and height of 0.6 cm, then left to dry in ambient air for 24 hours. The green compacts were then debinded by a thermal decomposition step at 803 K (530 °C) for 20 minutes under vacuum (10^{-3} torr). Upon debinding, the vacuum level was reduced to 10^{-5} torr, and the furnace was ramped to the sintering temperature at a rate of 5 K/minute. The sintering temperatures and soak times used in this study were 1473 K, 1498 K, and 1523 K (1200 °C, 1225 °C, and 1250 °C), and 10, 60, and 180 minutes, respectively. The temperature deviation in the furnace was measured to be ±5 K using a thermocouple located beside the compact. After the soaking period, the compacts were furnace cooled to room temperature. The compacts density was measured using the Archimedes method.[21] Preparation of the samples for microstructure observation was done using cold resin mounting under vacuum to ensure impregnation of the porous compact. The mounted samples were ground and polished using silicon carbide grinding papers (80, 200, 600 grit) and diamond suspension (9, 1 μm) on polishing cloths, respectively. A final polishing step was done with colloidal silica immediately followed by etching with Aqua Regia solution (3:1 HCl:HNO$_3$) for 3 to 20 seconds. The microstructure was observed using a Nikon light optical microscope, and grain size was measured using Clemex Vision image analysis software. A minimum of 300 grains were measured to compute the average grain size.

III. RESULTS AND DISCUSSION

A. Thermal Analysis

DSC was used to detect the melting events in the starting powder in order to identify the boundaries for the SLPS trials. A representative DSC trace is presented in Figure 2. As depicted, three thermal events were detected. First, two endothermic peaks measured at 1271 K and 1401 K (998 °C and 1128 °C) were attributed to the eutectic reaction γ + Laves $\rightarrow L$ and agree well with the data from Antonsson et al.[22] who measured a temperature range of 1433 K to 1348 K (1160 °C to 1075 °C) for this reaction during a cooling
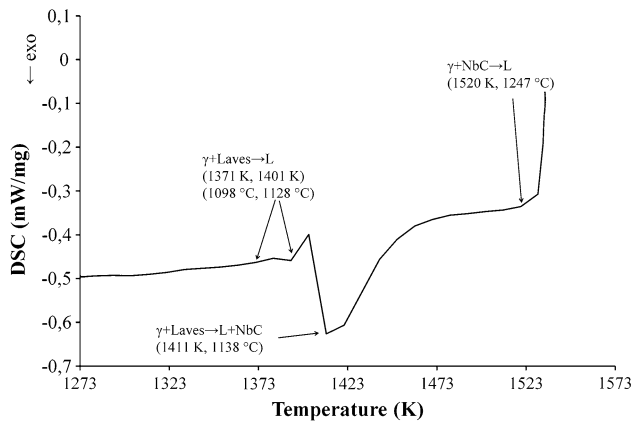
Fig. 2—DSC trace of the Inconel 718 powder between 1273 K and 1533 K (1200 °C and 1260 °C) scanned at 10 K/min.

Fig. 3—Solid fraction determined for Inconel 718 as a function of temperature by DSC measurement and by experimental observation.[22]

experiment. The second thermal event identified was the exothermic reaction γ + Laves $\rightarrow$ L + NbC occurring at 1411 K (1138 °C). Antonsson et al.[22] reported the formation of NbC carbides to occur at 1433 K (1160 °C), which is also in agreement with the current measurements. Finally, the endothermic peak, shown at 1520 K (1247 °C), is due to the eutectic reaction γ + NbC $\rightarrow$ L. This eutectic temperature is in line with the eutectic onset temperature found in the literature [1498 K to 1544 K (1225 °C to 1271 °C)].[22,23] The thermal events detected demonstrate that the current powders exhibit the characteristic melting events observed in Inconel 718. The small discrepancies observed between the reported temperatures and the experimental data are common for superalloys, and are explained by differences in alloying element content, segregation level, and dendrite arm spacing of the starting materials.[22] The data available in the literature were obtained with bulk Inconel 718, for which the grain size and segregation level are more important than for fine powder. As reported, the first melting event occurs at 1271 K (1198 °C), defining the SLPS regime lower boundary.

The DSC results were used to evaluate the liquid fraction developed in the Inconel 718 powder using Eq. [13]. Using the latent heat of fusion reported by Antonsson et al.[22] (241 kJ/kg) for all the melting events, the liquid fraction formed was calculated. The liquid fraction values obtained within the experimental limits of the available equipment are presented in Figure 3. The melting behavior of Inconel 718 powders is a non-equilibrium process. No experimental data of the liquid fraction formed during powder heating have been reported in previous work. However, Antonsson et al.[22] reported on the liquid fraction present during solidification of Inconel 718 calculated from DSC heat release and measured from the microstructure of 8 samples quenched at temperatures of 1597 K, 1593 K, 1567 K, 1566 K, 1516 K, 1461 K, and 1411 K (1324 °C, 1320 °C, 1294 °C, 1293 °C, 1243 °C, 1188 °C, and 1138 °C). Their reported experimental liquid fraction values are shown in Figure 3. As depicted, the current results are in agreement with Antonsson et al.'s[22] work. Moreover, Pandat™ (Computherm LLC, Madison,
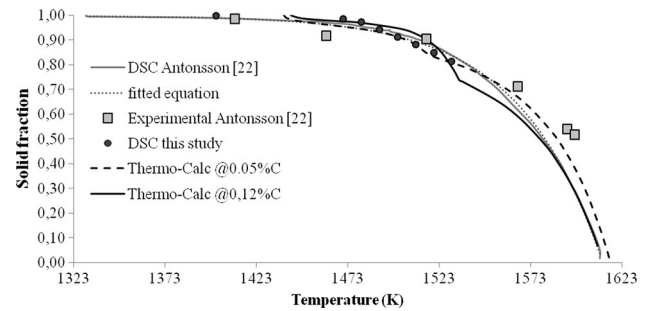
USA) software was used with the PanNickel database to assess the effect of binder carbon contamination on the liquid formation. The solid fraction of Inconel 718 at two carbon concentration of 0.05 and 0.12 pct was computed using nickel as the balance element, and the resulting melting curves are shown in Figure 3. The solid fraction is significantly modified by carbon contamination, especially at temperatures over 1540 K (1267 °C), where it decreases sharply for the 0.12 pct carbon concentration. The 1540 K (1267 °C) solid fraction obtained at 0.12 pct carbon is 6.8 pct lower than at 0.05 pct carbon, and the difference increases to 8.6 pct at a temperature of 1472 K (1199 °C). Carbon contamination from the binder or other sources modifies the sintering behavior of Inconel 718 by changing the equilibrium liquid fraction formation; however, the carbon contamination using ammonium alginate binder was shown to be negligible by Hajmrle.[24] In the current study, an exponential regression line fitting both DSC datasets obtained in this study and by Antonsson et al.[22] was used to interpolate the liquid fraction for all temperatures needed to cover the SLPS regime.

B. Densification and Microstructure Evolution

The densities measured for each sintering experiment are presented in Figure 4, along with reported densities from other works. As expected, both time and temperature were found to positively influence the densification. The densification is more efficient at 1523 K (1250 °C) with a density of 89.9 pct after 10 minutes compared to 71.1 and 57.7 pct after 10 minutes at 1498 K and 1473 K (1225 °C and 1200 °C), respectively. This difference is due to the increase in liquid fraction; the calculated liquid fractions are 4.7 pct for 1473 K (1200 °C), 8.1 pct for 1498 K (1225 °C), and 14.0 pct at 1523 K (1250 °C), respectively. The samples were not distorted after sintering meaning they still had enough rigidity to sustain their own weight.

The last experimental data needed to calibrate the SLPS model are the grain growth during sintering. A typical micrograph of etched Inconel 718 sintered at 1523 K (1250 °C) for 10 minutes is shown in Figure 5, and average grain size was obtained for each sample as presented in Figure 6. As depicted, the results are in agreement with previously published studies.
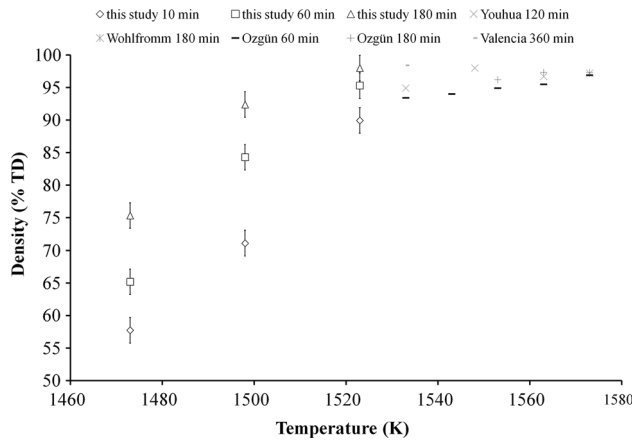
Fig. 4—Sintered density measured in this study and from other works.[6,8,10,11] The error bars represent the standard deviation obtained from the measurement of 3 repeated samples sintered at 1523 K (1250 °C) for 3 h, other results are from single experiments.
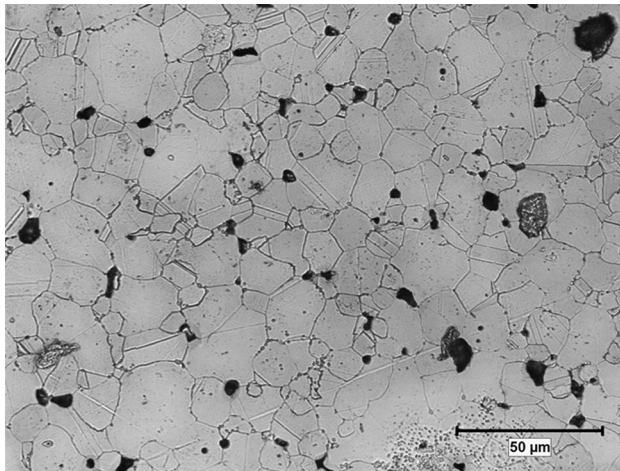

Fig. 5—Typical micrograph of etched Inconel 718 sintered at 1523 K (1250 °C) for 10 min.
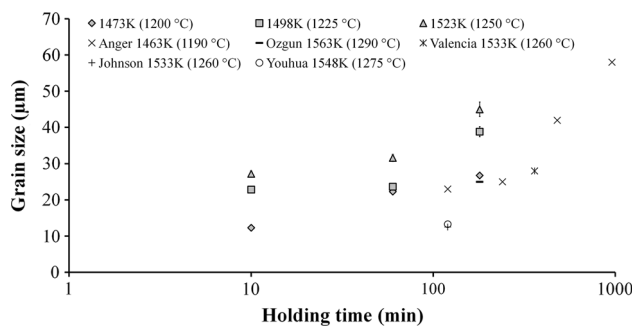

Fig. 6—Average grain size data obtained in this study and from other works,[5,6,8,11,25] the error bars are the 95 pct confidence interval on the average grain size.

The grain size measured at 1473 K (1200 °C) is in line with the results obtained by Anger and Hajmrle[25] at 1463 K (1190 °C) for similar powder particle size. However, the mean particle size used in other studies
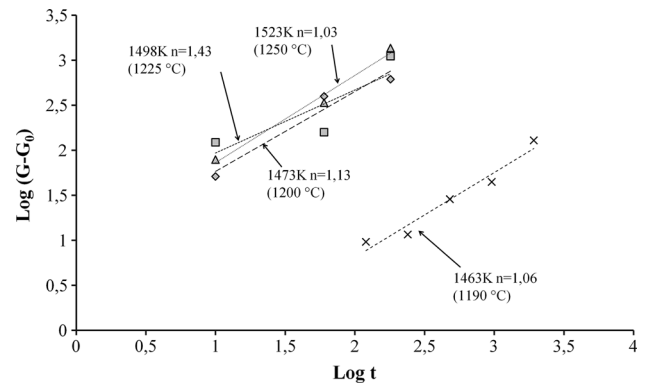

Fig. 7—Log–log plot used to determine the grain growth exponent (n) measured in this study and by Anger.[25]

varies from 7.4 to 15 μm, which is one-half to one-third of the average particle size used in this study and explains the lower grain size obtained in other studies. Grain growth during sintering is often described by the usual coarsening model as expressed in Eq. [14]:

$$G^n - G_0^n = kt, \qquad [14]$$

where G_0 is the grain size at the beginning of the isothermal hold, n is the grain growth exponent (usually $n \geq 2$[26]), k is the temperature dependant constant, and t is the isothermal time. The grain sizes in the current study and from the work of Anger and Hajmrle[25] were analyzed to determine the grain growth exponent in order to identify the grain growth mechanism occurring during SLPS; regression analysis of the grain size data is presented in Figure 7. Lack of completeness in the reported grain size and extent of studied processing parameters prevented the analysis of a larger number of works. As shown, the data are converging towards a grain growth exponent of 1, which is associated with partial pinning of the grain boundaries by the remaining porosity. This influence of the porosity on the grain growth also qualitatively fits the grain size measurement from others works, where smaller grain size were obtained for increased sintering conditions, as per their smaller starting particle size.

C. SLPS Model Prediction of Sintering and Distortion Onset for Inconel 718

The sintering results obtained in this work, as well as reported works carried out in a similar temperature range, exhibit typical SLPS behavior. The density increases steeply between temperatures of 1473 K to 1523 K (1200 °C to 1250 °C) due to the increasing liquid volume fraction that allows capillary forces to act on grains and fill voids between particles. As previously mentioned, the liquid fractions calculated for the samples sintered at 1473 K, 1498 K, and 1523 K (1200 °C, 1225 °C, 1250 °C) are 4.7, 8.1, and 14.0 pct, respectively. According to German,[16] the liquid fraction needed to achieve semisolid state is between 10 and 40 pct; when the liquid volume fraction is within this range, the compact is mushy (5 to 25 pct), whereas the

compact is considered rigid when the liquid fraction is lower (<5 pct). The mushy state refers to a semisolid structure where the liquid cannot flow within the solid skeleton. The overlap between mushy and semisolid state is related to the melt behavior of different materials. Densification is still assisted by the presence of <10 pct liquid fraction. However, as demonstrated for the samples sintered at 1523 K (1250 °C), the shrinkage drastically increases when the liquid fraction increases over 10 pct.

The sintering temperatures used in other studies mostly range from 1533 K to 1573 K (1260 °C to 1300 °C). The 1573 K (1300 °C) upper limit was reported by Wohlfromm[10] as the maximum temperature that could be used without distortion caused by slumping of the compact. In fact the liquid fraction predicted for 1573 K (1300 °C) is 42 pct which is larger than the 40 pct maximum liquid fraction defining the semisolid regime. At this liquid fraction content, most metals behave like fluids and distortion is expected.

To take into account the effect of microstructure (average particle size, average grain size) on the distribution of liquid in the compacts, Liu et al.[14] introduced a factor defined as the softening parameter (ξ). The definition of this parameter uses the liquid fraction and average grain size to determine the liquid film thickness as shown in Eq. [12]. The softening parameter for Inconel 718 was calculated for the current experimental data as well as for the available literature data using the average grain size measured at the end of sintering. The modeled curves of the softening parameter as a function of average grain size for each temperature used in this study and by other workers can be found in Figure 8, superimposed with the softening parameter calculated for the corresponding experimental data points.

The softening parameter increases with average grain size, and more so increases with temperature. The distortion threshold was determined according to the results of Wohlfromm et al.[10] who found the maximum temperature of sintering without distortion for 5 mm height Inconel 718 samples was 1573 K (1300 °C) with an average grain size of approximately 20 μm. As seen in Figure 8, at 1573 K (1300 °C), a slight increase in average grain size over 20 μm during the sintering of 5 mm height samples can potentially cause distortion because the softening parameter crosses the distortion threshold for this geometry. The onset of distortion estimated from the experimental data of Wohlfromm[10] is indicated on the graph at a softening value of 0.66 $\mu m^{1/3}$. Interestingly, Ozgun et al.[6] reported distortion at 1573 K (1300 °C) but not at 1563 K (1290 °C) meaning that the average grain size they obtained was probably higher than the threshold for their sample geometry (not described by the author). Finally, to determine the onset of sintering, we defined its occurrence as when the shrinkage (defined as the linear dimensional change $\Delta L/L_0$) reached 1 pct. Based on the average grain size and temperature observed at the onset of sintering by Hajmrle and Anger[4,25] and in this study, a softening parameter at the onset of sintering of 0.05 $\mu m^{1/3}$ was computed using Eq. [12]. Since the softening parameter does not take into account the particle size, it is assumed that the model holds for different powder feedstock. Moreover, the data obtained in the present study agree with Hajmrle and Anger[4,25] which support the use of different data sources to define the model parameters. Using the experimental values of $\xi_{distortion}$ and ξ_{onset} in Eqs. [10] and [11], along with the experimentally determined viscosity of liquid Inconel 718[27] and a dihedral angle of 30 deg, the set of equations was solved to find α and σ_{ss}. To simplify the calculations, the average viscosity of Inconel 718 between 1473 K and 1573 K (1200 °C and 1300 °C) was considered constant.[27] All the parameters used in the calculations are given in Table II. The mechanical strength of solid-solid contacts was found to be
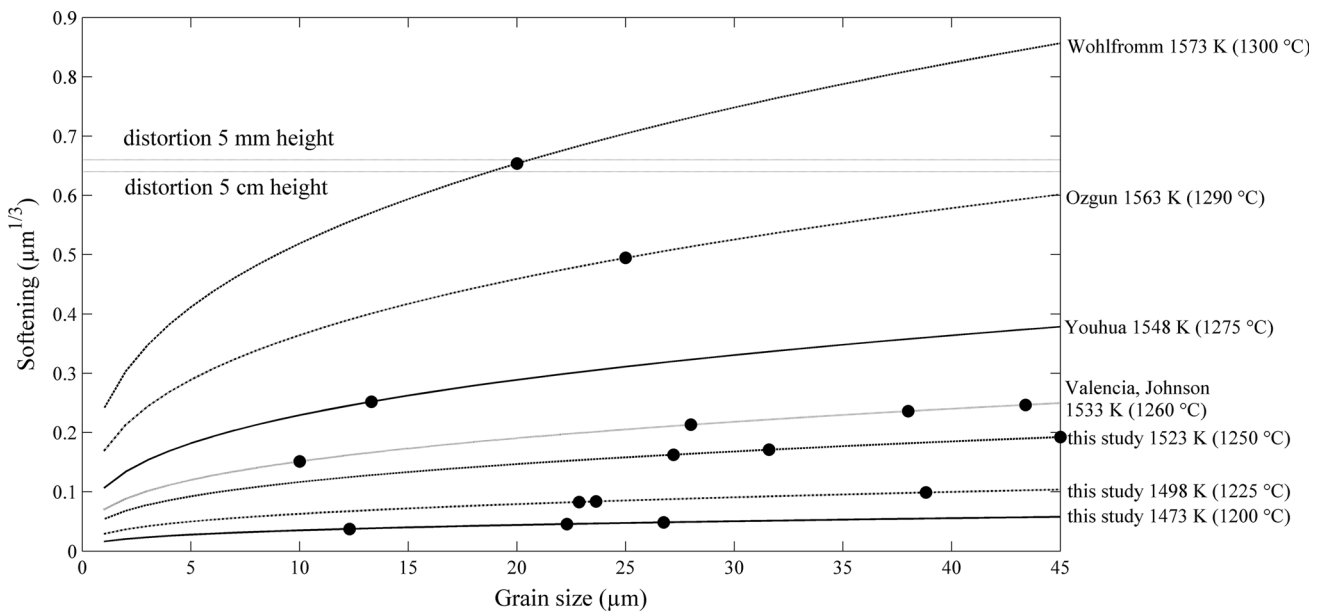

Fig. 8—Softening parameter calculated for the experimental conditions used in this study and in other works.[5,6,8,10,11]

Table II. Parameters Used to Compute $\xi_{distortion}$ and ξ_{onset}

Viscosity (mPa s)	Dihedral Angle (deg)	Wetting Angle (deg)	Liquid Vapor Surface Energy (J)	Green Density	Sintering Onset Density	Distortion Onset Density	Height (m)
9[27]	30[14]	0[16]	1.5[16]	0.6	0.61	1	0.005[10]

0.169 MPa, which is a reasonable value given that the yield strength of semisolid systems usually ranges between 0.00001 and 100 MPa.[16] The velocity constant was found to be 3.3×10^5 m/s. This model permits the prediction of $\xi_{distortion}$ and ξ_{onset} for varying compact geometry and powder particle size.

As seen from the data presented in Figure 8, sintering Inconel 718 at temperatures higher than 1563 K (1290 °C) can be problematic if the furnace has poor temperature control or long sintering time is used (increase in grain size) because the conditions are very close to the onset of distortion. However, simulations with various sample heights did not show a strong effect of this parameter on the distortion onset. The distortion onset for a 5 mm height sample occurred at 0.66 $\mu m^{1/3}$, whereas it occurred at 0.64 $\mu m^{1/3}$ for a 5 cm height part. This change could be enough to cause slumping during sintering at 1573 K (1300 °C); however, the softening parameter for sintering done at 1563 K (1290 °C) seems to remain below the critical values for the range of grain sizes considered in this study.

IV. CONCLUSION

This study proposes a SLPS model, built from a wide range of experimental data, to predict a process window for the sintering of Inconel 718. The model allows prediction of the distortion of a part for a given set of process parameters and part geometry (height). Specifically, the grain growth exponent was found to be between 1.03 and 1.43 in the temperature range between 1473 K and 1523 K (1200 °C and 1250 °C), and the softening parameter for distortion onset was computed according to the distortion data available in the literature. Using the grain growth relation will allow the prediction of distortion during sintering at temperatures higher than 1573 K (1300 °C). This model will be essential in optimizing the sintering of PIM or BJ - AM Inconel 718 parts.

ACKNOWLEDGMENT

NOMENCLATURE

F_C	Coverage of solid grains by liquid
V_L	Liquid volume fraction
ϕ	Dihedral angle (degrees)
C_{SS}	Contiguity of the semisolid structure
δ	Thickness of the grain boundary liquid film (m)
G	Average grain size (m)
R	Resistance to movement between two grains (N)
η_L	Viscosity of the liquid phase (mPa s)
v	Relative velocity of the two grains (m/s)
A	Area of the grain faces (m^2)
σ_{SS}	Resistance of the solid contacts between grains (MPa)
α	Constant (m/s)
γ_{LV}	Liquid–vapor surface energy (J)
θ	Wetting angle (degrees)
D	Mean particle diameter (m)
ρ	Relative density
F_G	Shear force caused by gravity (N)
F_{bond}	Bond strength between two grains (N)
h	Height (m)
$Q_{melting}$	Measured heat of fusion (J)
m_{sample}	Sample mass (kg)
ΔH	Latent heat of fusion (kJ/kg)
n	Grain growth exponent
k	Temperature dependant constant (m^n/s)
t	Time (s)
ξ_{densif}	Criterion for the onset of sintering
$\xi_{distort}$	Criterion for the onset of distortion
ξ	Softening parameter ($\mu m^{1/3}$)

REFERENCES

1. E. Sachs, M. Cima, P. Williams, D. Brancazio, and J. Cornie: *J. Eng. Ind*, 1992, vol. 114, pp. 481–88.
2. J.M. Contreras, A. Jiménez-Morales, and J.M. Torralba: *Powder Metall.*, 2008, vol. 51, pp. 103–06.
3. P.A. Davies, R. Dunstan, R. Howells, and A.C. Hayward: *Adv. Powder Metall. Part. Mater.*, 2003, vol. 8, pp. 8–12.
4. K. Hajmrle and R. Angers: *Int. J. Powder Metall. Powder Technol.*, 1980, vol. 16, pp. 255–57.
5. J.L. Johnson, L.K. Tan, P. Suri, and R.M. German: *Proceedings of PM2Tec 2004*. 2004, pp. 89–101.
6. O. Özgün, H.O. Gulsoy, R. Yilmaz, and F. Findik: *J. Alloys Compd.*, 2013, vol. 576, pp. 140–53.
7. J. Sicre-Artalejo, F. Petzoldt, M. Campos, and J.M. Torralba: *Int. J. Powder Metall.*, 2008, vol. 44, pp. 35–43.
8. J.J. Valencia, J. Spirko, and R. Schmees: *4th International Symp. Superalloys 718, 625, 706 Var. Deriv.* 1997, pp. 753–62.
9. R. Schmees, J.R. Spirko, and J. Valencia: *5th Int. Conf. Adv. Part. Mater. Processes*. 1997, pp. 493–99.
10. H. Wohlfromm, A. Ribbens, J. Maat, and M. Blomacher: *Proceedings Euro PM2003 Congr. Exhib.* 2003, vol. 3, pp. 207–15.
11. H. Youhua, L. Yimin, H. Hao, L. Jia, and T. Xiao: *Rare Met. Mater. Eng.*, 2010, vol. 39, pp. 775–80.
12. A. Bose, J.J. Valencia, J. Spirko, and R. Schmees: *Adv PM Part Mater*, 1997, vol. 3, pp. 18099–112.
13. W. Betteridge and S.W.K. Shaw: *Mater. Sci. Technol.*, 1987, vol. 3, pp. 682–94.

14. J. Liu, A. Lal, and R.M. German: *Acta Mater.*, 1999, vol. 47, pp. 4615–26.
15. R.M. German: *Mater. Trans.*, 2001, vol. 42 (7), pp. 1400–10.
16. R.M. German: *Metall. Mater. Trans. A*, 1997, vol. 28A, pp. 1553–67.
17. Y.X. Liu, R. Tandon, and R.M. German: *Metall. Mater. Trans. A*, 1995, vol. 26A, pp. 2423–30.
18. J. Campbell: *Metallography*, 1971, vol. 4, pp. 269–78.
19. Y.X. Liu, R. Tandon, and R.M. German: *Metall. Mater. Trans. A*, 1995, vol. 26A, pp. 2415–22.
20. M. Starink: *Int. Mater. Rev.*, 2004, vol. 49, pp. 191–226.
21. Metal Powder Industries Federation: *Method for Determination of Density of Compacted or Sintered Powder Metallurgy Products,* MPIF Standard No. 42. Metal Powder Industries Federation, Princeton, NJ, 2002, pp. 59–62.
22. T. Antonsson and H. Fredriksson: *Metall. Mater. Trans. B*, 2005, vol. 36B, pp. 85–96.
23. Y.C. Fayman: *Mater. Sci. Eng.*, 1987, vol. 92, pp. 159–71.
24. K. Hajmrle: *Forgeage d'ébauches poreuses d'Inconel 718 préparées par coulage en moule poreux et frittage*. S.l: Université Laval, 1978. p. xxii, 413 f.
25. R. Angers and K. Hajmrle: *Scr. Metall.*, 1980, vol. 14, pp. 577–81.
26. H. Hu and B.B. Rath: *Metall Trans*, 1970, vol. 1, pp. 3181–84.
27. N. Saunders, U.K.Z. Guo, X. Li, A.P. Miodownik, and J.P. Schillé: *JOM*, 2003, vol. 55, pp. 60–65.